White Blood Cells Detection from Unstained Microscopic Images using Modified Watershed Segmentation

Lina Lina, *Member IAENG*, David Reynaldo, Danny Danny, and Arlends Chris

Abstract—Detection of white blood cells on a microscope slide using image processing technology has been widely used in health-related research for over a decade. However, most of the proposed research is performed on blood cells with color-stained images. These images are obtained by capturing microscope slide images that have been previously stained with various substances. Unfortunately, this task is very rigorous and time—and—cost inefficient. This study attempted to eliminate the staining phase in the preprocessing stage and aimed to develop an automatic system to detect white blood cells from unstained microscopic images. A modification of the watershed segmentation method was applied to the developed system to differentiate white blood cells from other cells. First, a preprocessing stage which applies various image enhancement techniques was performed to improve the image quality, and the red blood cell areas were subsequently eliminated using the modified watershed segmentation method. The final result was determined by the area size and aspect ratio of the segmented area. Experimental results showed that the average detection accuracy for locating white blood cells from unstained images was 65.42%, while 94.82% average detection accuracy was achieved for color-stained images. Several experiments using the same datasets were also executed by applying the Convolutional Neural Network (CNN) method. The obtained average detection accuracies for the CNN method were 65.33% and 74.85% for the unstained images and the color-stained images, respectively. The comparison of the two methods showed that the developed system can effectively perform blood cells detection without using the color-stained images.

Index Terms—Segmentation, White blood cell, Unstained microscopic image, Area detection.

L. Lina is an Associate Professor of Computer Science Department, Tarumanagara University, Jakarta, 11440 Indonesia (corresponding author to provide phone: +62-21-567-6260; fax: +62-21-5694-1924; e-mail: lina@untar.ac.id).

D. Reynaldo is a research assistant of Pattern Recognition research laboratory, Computer Science Department, Tarumanagara University, Jakarta, 11440 Indonesia (e-mail: 535150044@stu.untar.ac.id).

D. Danny is a research assistant of Pattern Recognition research laboratory, Computer Science Department, Tarumanagara University, Jakarta, 11440 Indonesia (e-mail: 535170091@stu.untar.ac.id).

A. Chris is an Assistant Professor of Medical Faculty, Tarumanagara University, Jakarta, 11440 Indonesia (e-mail: arlendsc@fk.untar.ac.id).

I. INTRODUCTION

WHITE blood cells constitute the human blood cell compositions and play major roles in the human immune system. The analysis of the white blood cell has become one of the main procedures for medical diagnosis. Therefore, several types of research have been conducted to integrate new technologies for automatic detection and analysis of blood cells. Several works put focus on detecting the white blood cells using some image pre-processing techniques, such as processing the color features [1][2], scaling and smoothing of cell images [3], correcting color space of cells [4], removing noise using convolution masks [5], performing morphological analysis [6], extracting color from mean intensity of the cell images [7], enhancing image color of the blood cells [8], and implementing various image domain transformation [9][10]. Moreover, various methods have been proposed to develop a blood cell detection system, such as the location transformation [11], the Active Contour Model [12][13], and the Edge Strength Cue [14].

Recently, artificial neural network and deep learning methodologies are preferred when performing various health-related analysis, such as blood cell detection using the modified deep residual neural network [15] and the combination of neural network and Support Vector Machine [16]. A popular method of deep learning is the Convolutional Neural Network (CNN). CNN has been employed for various applications, such as leukemia diagnosis [16][17], blood cell recognition [18][19][20], segmentation of pigmented skin lesion [21], and lesion-infection detection of Covid-19 [22].

Related work by Kutlu et. al. [23] showed successful classifications of the white blood cell types using low-resolution images The results of the classification system showed that the CNN method was more accurate than the SVM method. Another work that used the deep learning approach to peripheral leukocyte recognition was conducted by Wang et al. [24]. In their proposed system, the Single Shot Detector (SSD) method and the You Only Look Once (YOLO) method were applied. The system was claimed to have good performance with YOLO outperforming the SSD.

A common property of the existing research is in the use of stained images as input. The staining process is usually performed manually by laboratory technicians to color the blood smear on the microscope slides prior to the image capturing stage. A stained blood smear is subsequently photographed to produce digital blood cell images. The
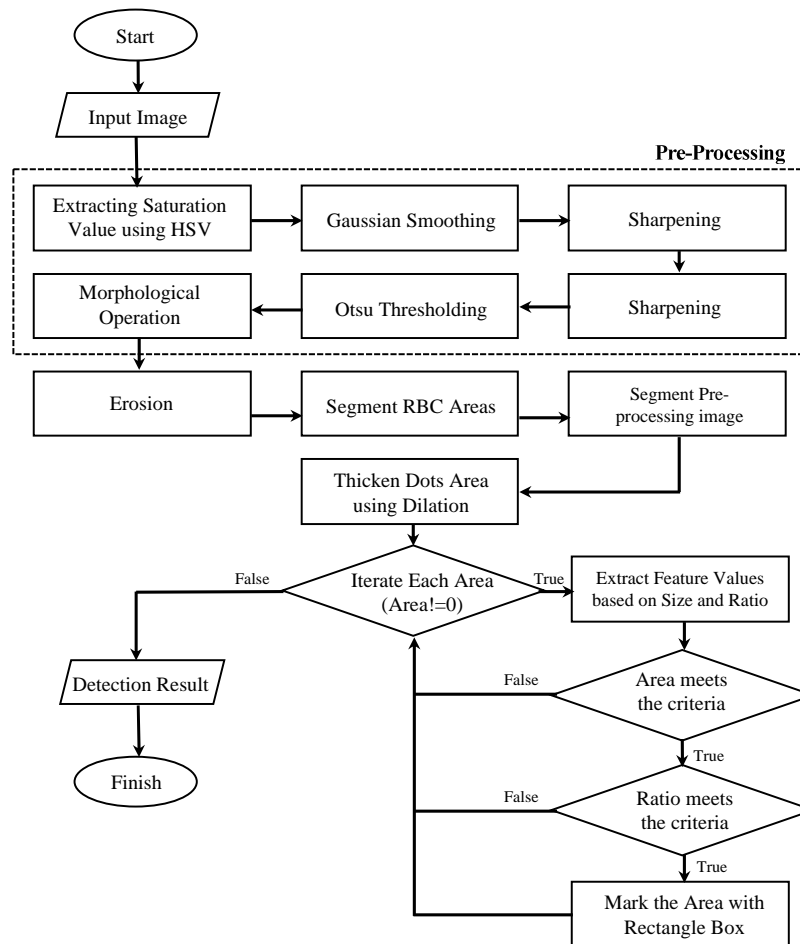
Figure 1. Proposed detection system from unstained blood cell images

blood cell types in the stained images can be distinguished easily by both human and computer vision. Thus, they could give high accuracy to the system. However, a major disadvantage of using stained images in blood cell detection or recognition systems is the inefficiency of the image manufacturing process.

In this study, the white blood cell detection system is performed on the unstained microscopic images. The unstained images are almost transparent and unrecognizable to the human eyes. The input of the proposed system is unstained microscopic images, which contain red and white blood cells. Thus, the image preparation step in the proposed system is more efficient because it does not require coloring process of the microscope slides. The main process for white blood cell detection consists of two stages, i.e., the image enhancement subsystem and the image segmentation using the modified watershed method. The target of the proposed system is to obtain the white blood cell area and mark them automatically. This study is organized as follows: the proposed system with a block diagram is discussed in Section 2, followed by experimental results in Section 3, and conclusion in Section 4.

II. PROPOSED WORK

The proposed system is designed to receive input of microscopic images from unstained blood cells. In the first stage, various image enhancement procedures, such as color extraction, image smoothing, image thresholding, and morphological operations are performed. Subsequently, the main segmentation process is conducted by applying the modified watershed segmentation method to estimate the positions of the white blood cell areas. The final segmentation decision is obtained by matching the prediction area to a certain size and ratio criteria. The block diagram of the proposed system is presented in Fig. 1.

A. Image Enhancement

In the first stage, several image enhancement methods are performed to improve the image quality and ensure the display of texture features. Fig. 2(a) shows the input sample of an unstained microscopic image in RGB domain. Because the cell areas in the input image are quite invisible, a color domain transformation of the input images is necessary. In this study, the RGB images are transformed to HSV to expose the color features of the blood cells. Fig. 2(b) shows the image result in HSV color domain.

In HSV color domain, the red blood cell areas are exposed perfectly. However, the white blood cell areas remain concealed. In this stage, the Saturation Value scores in HSV color space are extracted to obtain the texture. The empty spaces with shallow dots in Fig. 2(b) are the possible white blood cell areas.

Furthermore, the image smoothing and sharpening processes are conducted to eliminate additional noise and sharpen the texture of the blood cells. The popular Gaussian kernel and Laplacian kernel are subsequently applied.
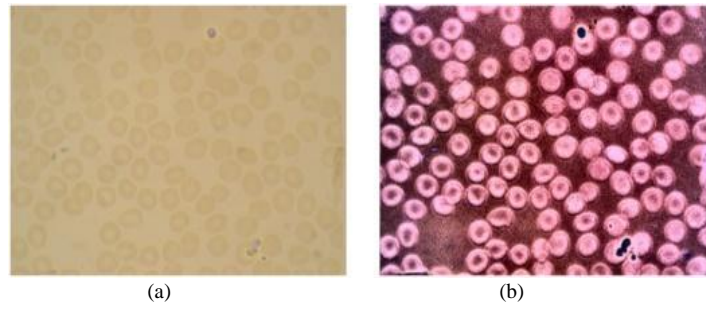
Figure 2. Image samples of unstained microscopic images in (a) RGB, (b) HSV
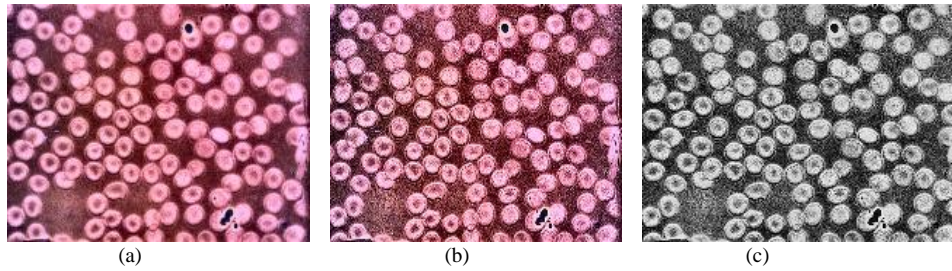

Figure 3. Image samples after (a) smoothing, (b) sharpening, and (c) grayscaling

The general formula for Gaussian kernel is as follows:

$$G(x, y) = \frac{1}{2\pi\sigma^2} e^{-\frac{x^2+y^2}{2\sigma^2}} \qquad (1)$$

where $G(x,y)$ is the Gaussian kernel in (x,y) position and σ is the deviation standard of the Gaussian distribution. After the smoothing and sharpening steps, the image result is then converted into a grayscale image to ensure a faster process. The image smoothing, sharpening, and grayscaling samples are shown in Fig. 3.

Additionally, a thresholding process is conducted to convert grayscale images into binary images. In this study, the Otsu method which can automatically determine the threshold value based on the histogram data of the image is performed. The Otsu thresholding algorithm begins with the construction of the image's histogram. Based on the obtained histogram intensity, the probability of each pixel P_i is calculated using the following equation:

$$P_i = \frac{n_i}{N} \qquad (2)$$

where n_i is the number of pixels with i intensity and N is the total number of pixel in the image. The cumulative sum $\omega(k)$ and the cumulative mean $\mu(k)$ for each gray level values are then calculated using (3) and (4), respectively, as follows:

$$\omega(k) = \sum_{i=0}^{k} p_i \qquad (3)$$

$$\mu(k) = \sum_{i=0}^{k} i.p_i \qquad (4)$$

After processing the values for each pixel intensity, the between class variance is calculated by the following equation:

$$\sigma_B^2(k) = \frac{[\mu_T \omega(k) - \mu(k)]^2}{\omega(k)[1 - \omega(k)]} \qquad (5)$$

where μ_T is input using this formula:

$$\mu_T = \sum_{i=0}^{L-1} i.p_i \qquad (6)$$

Next, the threshold value T is defined according to the maximum value from (5). Finally, a general comparison to the defined threshold value is applied to the whole image area using the following equation:

$$G(x, y) = \begin{cases} ? & \text{if } f(x,y) > T \\ ? & \text{if } f(x,y) \leq T \end{cases} \qquad (7)$$

The image sample result of Otsu thresholding is shown in Fig. 4(b). The morphological operation is a process using certain mathematical equations on a series of pixels to improve aspects of shapes and structures. The main purpose of implementing morphological operations in this stage is to fill the holes and empty spaces inside a cell area using dilation; or to remove small objects that do not constitute a white blood cell using erosion.

The dilation step is also known as a thickening process. It is often used to combine background points into an object based on the defined structuring element (SE). In this proposed system, a dilation operation is used to thicken the red blood cell areas to become one intact region and to combine the dots area, which possibly is a segment of a white blood cell. The dilation operation follows this formula:

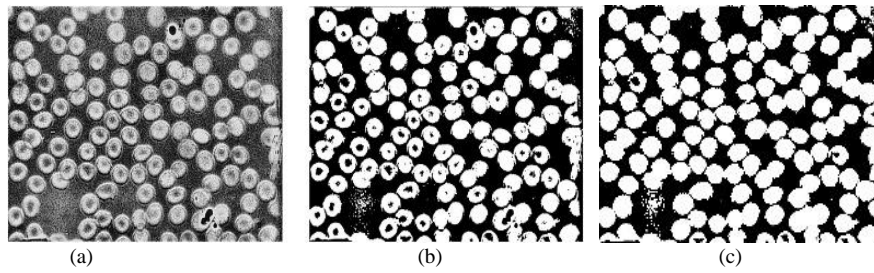$$g(x, y) = f(x, y) \oplus SE \qquad (8)$$

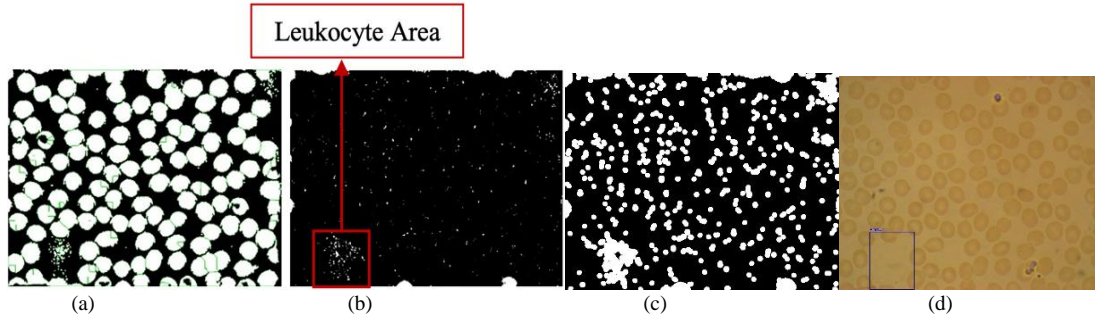Figure 4**.** Image samples of (a) grayscaling, (b) Otsu thresholding, and (c) morphological processing

Figure 5. Image samples of (a) morphological processing, (b) watershed segmentation, (c) dilation process, and (d) the final detection result

Another operation used in this study is erosion, which implements the following equation:

$$g(x, y) = f(x, y) \otimes SE \qquad (9)$$

Erosion is the opposite of the dilation operation. Erosion is used to delete or reduce pixels or size of an object. In this proposed system, the erosion process is expected to remove noises and eliminate speckled areas before the segmentation stage is carried out. The final result of both the dilation and erosion steps is depicted in Fig. 4(c).

A. Image Segmentation

After implementing the image enhancement techniques, the segmentation process is conducted based on the watershed transformation method. The watershed transformation method is a powerful region-based segmentation tool, which combines the region growing and the edge detection techniques to partition the image into two different sets, i.e., the object and the background.

The main concept of the watershed transformation is to assume that an image is a three-dimensional form, consisting of the pixel position (x, y) and the color level z. The positions of x and y are set to be the base field, while the position of z becomes the height. If the pixel color is white, then the z value has the maximum height; while if the pixel color is similar to black, the z value has the minimum height (zero score).

In the detection stage, the watershed segmentation method is applied on the preprocessed images which have been eroded using the erosion operation. The target of the detection step is to detect the areas of the white blood cells. The detection results are then marked and stored in a new array. The marked positions are subsequently used to segment the original input image. Thus, the results obtained from this process are image-patches which contain only the white blood cell areas.

Before implementing the watershed segmentation algorithm, some parameters need to be assigned to the system. Let M_1, M_2, ..., M_R denote the coordinates in the regional minima of an image $g(x, y)$; where $g(x, y)$ is the pixel value of coordinate (x, y). Then, define $C(M_i)$ as the coordinates associated with regional minimum M_i. Finally, let $T[n]$ be the set of coordinates (s, t) for which $g(s, t) < n$ as follows:

$$T[n] = \{(s, t) \mid g(s, t) < n\} \qquad (10)$$

Then, compute the following formula:

$$C_n(M_i) = C(M_i)T[n] \qquad (11)$$

If (x, y) is in $C(M_i)$ and $T[n]$, then $C_n(M_i) = 1$ at location (x, y); otherwise $C_n(M_i) = 0$. Continue with setting an incremental value of n where $n = n + 1$.

Moreover, derive the set of connected components in $T[n]$ denoting as Q. For each connected component q in $Q[n]$:
1) if the intersection of q with $C[n-1]$ is empty, the connected component q is incorporated into $C[n-1]$ to form $C[n]$ because it represents a new minimum.
2) if the intersection of q with $C[n-1]$ contains one connected component of $C[n-1]$, the connected component q is incorporated into $C[n-1]$ to form $C[n]$ because it lies within the regional minimum.
3) if the intersection of q with $C[n-1]$ contains more than one connected component of $C[n-1]$, the points of the ridge which separates two or more parts should be located. Finally, construct $C[n]$ according to equation 11 and set $n = n + 1$.

The above steps are repeated until n reaches the maximum value.
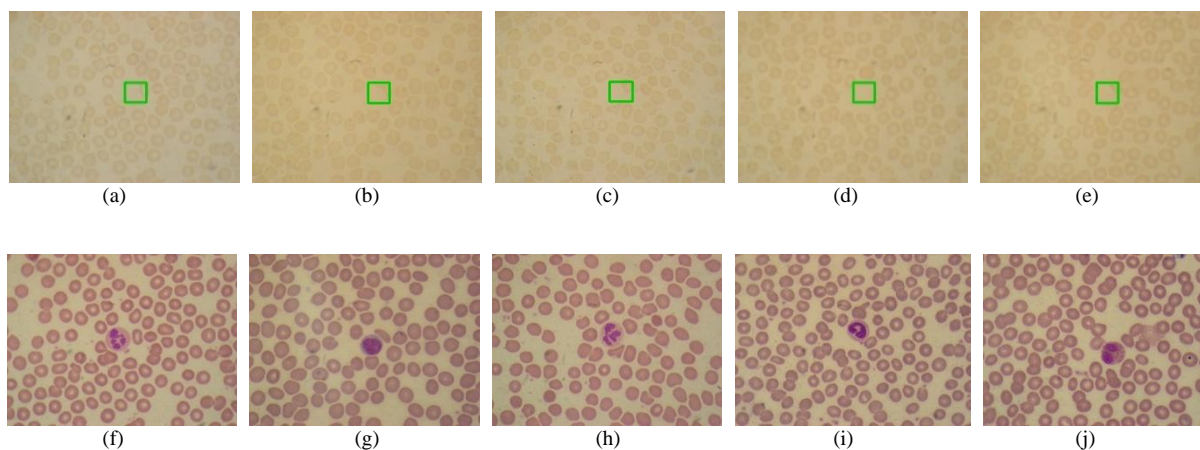
Figure 6. Image samples of (a) morphological processing, (b) watershed segmentation, (c) dilation process, (d) the final detection result

In this study, a modified watershed segmentation method is introduced to enable the implementation of the algorithm using a binary image input. First, the binary image is transformed into a gradient image by calculating the distance between pixels using the Euclidean Distance Transform (EDT). The formula for calculating EDT is as follows:

$$D = \sqrt{(x_1 - y_1)^2 + (x_2 - y_2)^2} \qquad (12)$$

The result of the EDT is a grayscale image that is similar to the input image, except that the gray level intensity of points inside the foreground regions are changed. After this operation, the resulting images are used as input in watershed segmentation using the algorithm described above. The result sample of the modified watershed segmentation is depicted in Fig. 5(b).

The last step is to determine whether the resulted dot areas are white blood cells. For this purpose, a dilation formula is used to thicken the dots area to ensure the adjacent spotted object can be interconnected into one whole region. Moreover, two features are extracted, namely, 1) the area value of total non-zero pixels in a region, and 2) the aspect ratio of the selected area. The aspect ratio is calculated by comparing the width and height of the selected region.

For the whole image, each possible area is compared with predetermined threshold values. In this system, a threshold value range of $4450 < area_i < 11400$ and an aspect ratio value with range of $0.5 < ratio_i < 2.3$ are determined. These values are defined based on the average dimension of a white blood cell. Normally, the dimension of a white blood cell is bigger than the red blood cell size in a microscopic image. Using these criteria, the system determines whether the segmented area is a white blood cell or not. The developed system then marks the white blood cell area by constructing a rectangle box on the image. The image samples of the image segmentation process are shown in Fig. 5.

III. RESULTS AND DISCUSSION

To evaluate the performance of the proposed system, several experiments were conducted. The authors collected and built a novel database to provide a pairing set of the unstained and the color-stained images. Because the white blood cells in the unstained images are hardly detected by human eyes, it is necessary to verify the obtained results by comparing them to the stained version of the same locations. The developed database consisted of two datasets with the first dataset containing a microscopic image with unstained blood cell images, while the second dataset contained microscopic images with color-stained blood cell images, which follows a standard coloring procedure. The numbers of image proportion used in the experiments for each dataset are shown in Table I. From Table I, it can be observed that the training images for each dataset were different. However, the testing images were pairs of unstained and stained images of the same blood cell locations. Therefore, the same numbers of testing images for both datasets are presented in Table I. The total number of unstained images used in Dataset 1 was 458 images, which consists of 264 images for training and 194 images for testing. For Dataset 2, the system had 528 stained images for training and 194 stained images for testing.

Fig. 6 shows the paired image samples for each dataset. The samples of the unstained images are depicted in Figs. 6(a) and 6(e), while Figs. 6(f) and 6(j) show the samples of the stained images. It can be seen in Figs. 6(a) and 6(e) that for the unstained images, the locations of the blood cell areas were difficult to detect with the human eye. Thus, green rectangles were added to mark the white blood cell areas for easier visibility. However, in the experiments, only the plain version of the unstained images, with no green rectangle marks, were inputted into the system. On the contrary, the blood cells in the stained images were easily detectable by the human eye, as shown in Figs. 6(f) and 6(j). Thus, it is obvious that detecting white blood cell areas using stained images is easier and can achieve a fairly high degree of accuracy.

In the first experiment, we developed the white blood cell detection system using the modified watershed method. The developed system followed the steps depicted in Fig. 1 and used the dataset explained in Table I. The detection accuracy of the developed system was calculated based on the number of correctly detected images divided by the total number of images that have been tested. Note that there were occurrences where images had zero or more than one white blood cell; therefore, the system was designed to detect more than one white blood cell area in an image. The white blood cell detection accuracy and the average processing time for the two datasets are shown in Table II.

Meanwhile, the detailed detection accuracy for each white blood cell type along with its image sample are shown in Table III.

Table I. Number of image proportion used in the experiments

Data	Dataset 1 – unstained images	Dataset 2 – stained images
Train	264	528
Test	194	194

Table II. Detection accuracy of the proposed system

Scenario	Detection Accuracy (%)	Average Time (sec)
Dataset 1 – Unstained images	65.72	0.515
Dataset 2 – Color-stained images	94.82	0.502

Based on Table II, the proposed system achieved 65.72% detection accuracy for Dataset 1 for the unstained blood cell images, with an average detection time of 0.515 seconds, while the experimental result on Dataset 2 shows a detection accuracy of 94.82% for the proposed system detecting the color-stained images. The average processing time for Dataset 2 is 0.502 seconds.

Table III shows the detection accuracy and image sample of each white blood cell type. The detection accuracy obtained for Neutrophil was 52.63%, 83.33% for Eosinophil, 100% for Basophil, 75% for Monocyte, and 17.65% for Lymphocyte. It is shown in Table III that Basophil and Eosinophil are white blood cell types that can be easily detected by the system. Meanwhile, Lymphocyte is the most difficult to be detected. A reason for the difficulty in detection of Lymphocyte is its dimension similarity with the red blood cells. Thus, the Lymphocytes are often left undetected.

Furthermore, we conducted some experiments using the Convolutional Neural Network (CNN) method. The CNN method was calculated after performing the same pre-processing stage as in the previous experiment, as shown in Fig. 2. Next, the bounding box regressors were used to locate white blood cells in suspected regions. In this experiment, the used datasets were similar, as explained in Table I. The CNN method consisted of the training stage and the testing stage. In the training stage, the CNN model was built using a pre-trained model, namely the VGG16.

The detailed configuration of the VGG16 architecture used in the experiment can be seen in Table IV. The applied VGG16 architecture had 18 layers, consisting of 13 convolution layers and 5 layers for pooling. The obtained model from the training stage was subsequently tested using various epoch configurations. Three different epoch configurations were determined— 30, 100, and 200 epochs. The purpose of this experiment was to determine the most optimal model for the trained dataset. During training, the samples were split into two internal sub-datasets: the actual training data and the validation data.

The accuracy and validation accuracy values for each epoch configuration for Training Set 1 (unstained images) and Training Set 2 (stained images) are shown in Fig. 7. The accuracy result for Training Set 1 with 30 epochs is depicted in Fig. 7(a), while Fig. 7(c) and Fig. 7(e) represent the results for Training Set 1 with 100 epochs and 200 epochs, respectively. Meanwhile, Fig. 7(b), Fig. 7(d), and Fig. 7(f) cover the accuracy results for Training Set 2 for 30 epochs, 100 epochs, and 200 epochs, respectively.

Table III. Detection accuracy and image sample of each of the white blood cell type using watershed segmentation
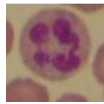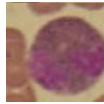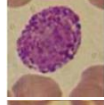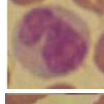
White Blood Cell Type	Image Sample	Detection Accuracy (%)
Neutrophil		52.63
Eosinophil		83.33
Basophil		100
Monocyte		75
Lymphocyte		17.65

Table IV. VGG16 Architecture

| Layer	Parameter Value	Output Shape
Conv2D	64, (3,3), Relu	(None,224,224,64)
Conv2D	64, (3,3), Relu	(None,224,224,64)
MaxPool2D	(2,2)	(None,112,112,64)
Conv2D	128, (3,3), Relu	(None,112,112,128)
Conv2D	128, (3,3), Relu	(None,112,112,128)
MaxPool2D	(2,2)	(None,56,56,128)
Conv2D	256, (3,3), Relu	(None,56,56,256)
Conv2D	256, (3,3), Relu	(None,56,56,256)
Conv2D	256, (3,3), Relu	(None,56,56,256)
MaxPool2D	(2,2)	(None,28,28,256)
Conv2D	512, (3,3), Relu	(None,28,28,512)
Conv2D	512, (3,3), Relu	(None,28,28,512)
Conv2D	512, (3,3), Relu	(None,28,28,512)
MaxPool2D	(2,2)	(None,14,14,512)
Conv2D	512, (3,3), Relu	(None,14,14,512)
Conv2D	512, (3,3), Relu	(None,14,14,512)
Conv2D	512, (3,3), Relu	(None,14,14,512)
MaxPool2D	(2,2)	(None,7,7,512)
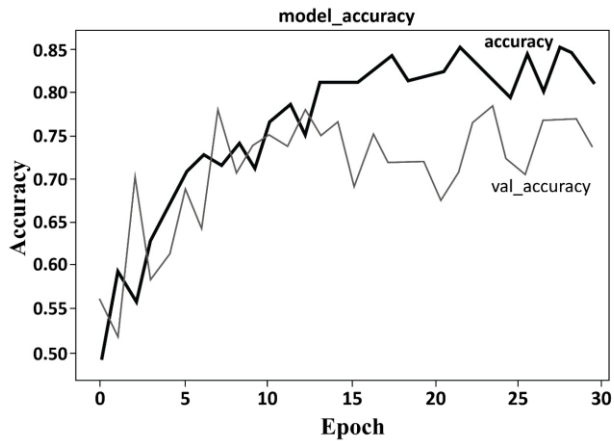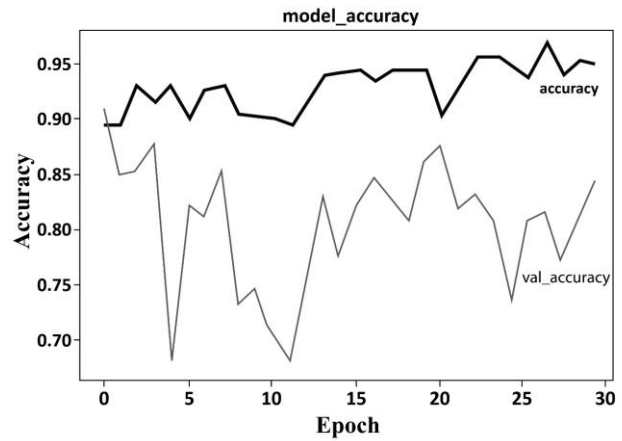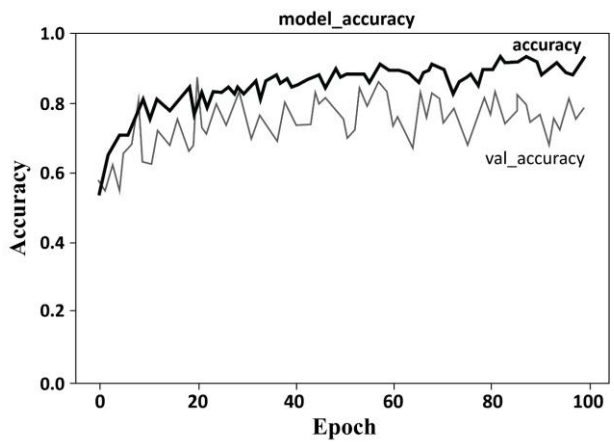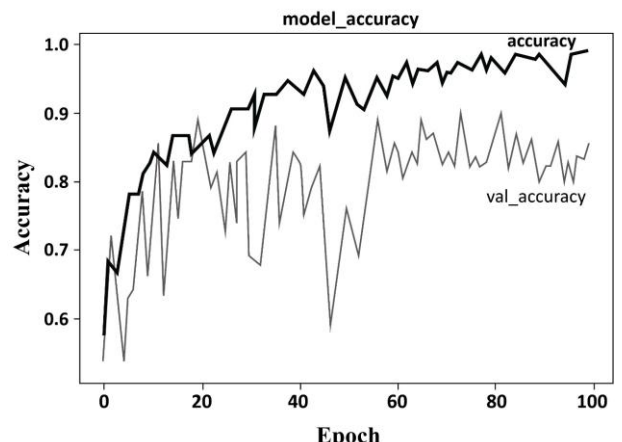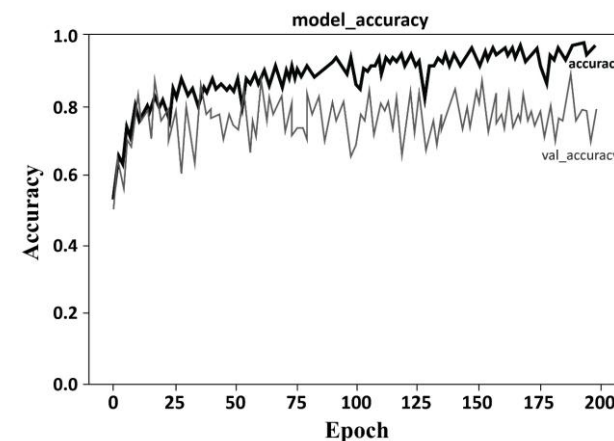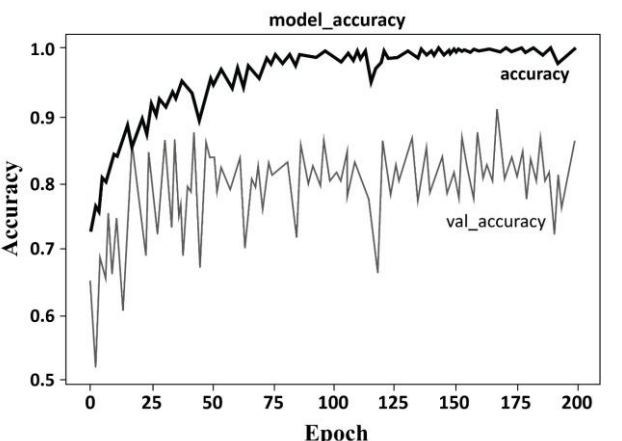
Figure 7. Accuracy and validation accuracy results for (a) Training Set 1 with 30 epochs, (b) Training Set 2 with 30 epochs, (c) Training Set 1 with 100 epochs, (d) Training Set 2 with 100 epochs, (e) Training Set 1 with 200 epochs, and (f) Training Set 2 with 200 epochs

Table V. Accuracy and loss values for various epoch configurations for Training Set 1 for unstained images

Epoch	Accuracy (%)	Loss	Validation Accuracy (%)	Validation Loss
30	79.89	0.3719	73.31	0.4853
100	92.75	0.2519	78.12	0.5476
200	96.79	0.0931	78.12	0.6744

Table VI. Accuracy and loss values for various epoch configuration for Training Set 2 for stained images

Epoch	Accuracy (%)	Loss	Validation Accuracy (%)	Validation Loss
30	94.89	0.2247	84.62	0.5289
100	99.05	0.0370	85.38	0.5132
200	100	0.0076	86.15	0.6162

Table VII. Accuracy values for various epoch configuration for both testing sets

Epoch	Accuracy (%)	
	Testing Set 1 – unstained images	Testing Set 2 – stained images
30	56.25	53.83
100	48.43	40.76
200	48.43	48.76

Table VIII. Results of Accuracy, Precision, Recall and F1-Score for both testing set

Dataset	Accuracy (%)	Precision (%)	Recall (%)	F1-Score (%)
Testing Set 1– unstained images	53.85	52.94	59.38	56.72
Testing Set 2 – stained images	54.69	59.24	69.23	60

Table IX. Detection accuracy of each white blood cell type using CNN

White Blood Cell Type	Detection Accuracy (%)	
	Testing Set 1 - unstained images	Testing Set 2 – stained images
Neutrophil	65	71.42
Eosinophil	66.67	60
Basophil	100	100
Monocyte	75	71.42
Lymphocyte	20	66.67

From Fig. 7, it can be observed that for both training sets, the results reached the highest accuracies with epoch 200, depicting a 96.79% accuracy value for unstained images and 100% accuracy value for stained images. The detailed accuracy and loss values for both training sets are presented in Tables V and VI. From Table V, it can be seen that the accuracy and validation accuracy results for Training Set 1 for unstained images increased along with the use of higher epoch values. On the contrary, the loss values decreased with the use of higher epoch values. These results fulfill the classic "high accuracy and low loss" behavior that we expected. However, the validation loss values slightly increased for higher epochs. These phenomena also occurred for Training Set 2 for stained images in Table VI.

Additionally, we conducted the experiments for images in Testing Set 1 and Testing Set 2. Table VII presents the accuracy rates for each epoch configuration for both testing sets. In contrast with the training results where the 200 epochs model gave the highest accuracy, for the testing set, the 30 epochs model achieved the best accuracy rates for both the unstained and stained test images. However the obtained accuracy values dropped significantly for all epoch configurations. The highest accuracy value for Testing Set 1 for the unstained images was 56.25%, while Testing Set 2 achieved a lower value of 53.83%. Considering the poor accuracy results for both testing sets, the model was suspected of overfitting.

Subsequently, the confusion matrix evaluation technique was implemented to measure the performance of the proposed system. Based on the results presented in Table VII, the experiments were conducted using the trained model with 30 epoch configurations, 64 batch sizes, and Adam's optimizer. The obtained results were then classified based on these categories: True Positive (TP), False Positive (FP), True Negative (TN), and False Negative (FN). The classification of each category was set as follows: TP is the number of images which contained white blood cells and were correctly detected, while FP is the number of images without any white blood cell, yet the system incorrectly detected some white blood cell areas. TN is the number of images with no white blood cells and no white blood cell area detection, and FN is the number of images which contained white blood cells, yet the system was unable to detect any area of the white blood cells. The results of each category were subsequently used for calculating the system's accuracy, precision, recall, and F1-score with the following formula:

$$Accuracy = \frac{TP + TN}{TP + TN + FP + FN} * 100\% \qquad (13)$$

$$Precision = \frac{TP}{TP + FP} * 100\% \qquad (14)$$

$$Recall = \frac{TP}{TP + FN} * 100\% \qquad (15)$$

$$F1\ Score = 2 \frac{Precision \times Recall}{Precision + Recall} * 100\% \qquad (16)$$

Table VIII shows the results of Accuracy, Precision, Recall and F1-Score for both testing sets. Based on the evaluation in Table VIII, Testing Set 1 which contained unstained images had an accuracy rate of 53.85%, a precision level of 52.94%, a recall rate of 59.38%, and an F1-score of 56.72%. Whereas for Testing Set 2, which processed the stained images, had a slightly higher accuracy rate of 54.69%, a precision level of 59.24%, a recall rate of 69.23%, and an F1-Score of 60%. Several factors, such as overfitting issue, nonoptimal layer configurations, and high similarity in size of the blood cells were suspected to cause the low accuracy score of the CNN method.

A detailed analysis of the detection accuracy of the system using CNN for each white blood cell type is presented in Table IX. Note that the accuracy values shown in Table IX singularly consider the detection results from images that contain white blood cells only because the images with no white blood cells could not be classified by its type. For Testing Set 1, the detection accuracy obtained for Neutrophil was 65%, 66.67% for Eosinophil, 100% for Basophil, 75% for Monocyte, and 20% for Lymphocyte; while for Testing Set 2, the achieved accuracy was 71.42% for Neutrophil, 60% for Eosinophil, 100% for Basophil, 71.42% for Monocyte, and 66.67% for Lymphocyte. A similar phenomenon can be seen from the results obtained from the developed system using the modified watershed segmentation method and the CNN method that presented the lowest detection accuracy for Lymphocyte. Based on the experimental results shown in Tables III and IX, it is shown that the developed system using the modified watershed algorithm obtained similar results to that of the CNN method for the same testing data. Both methods in the proposed system provide an effective means of performing blood cells detection without employing the staining process.
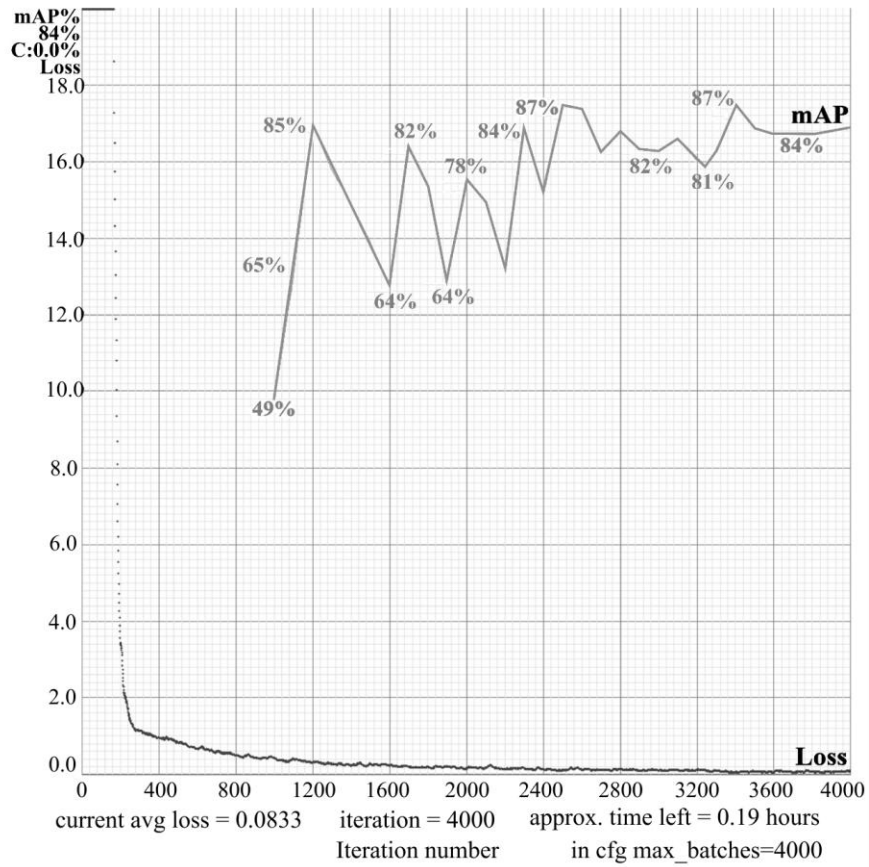
Figure 8. Accuracy and loss values for various epoch in testing set 1 – unstained images
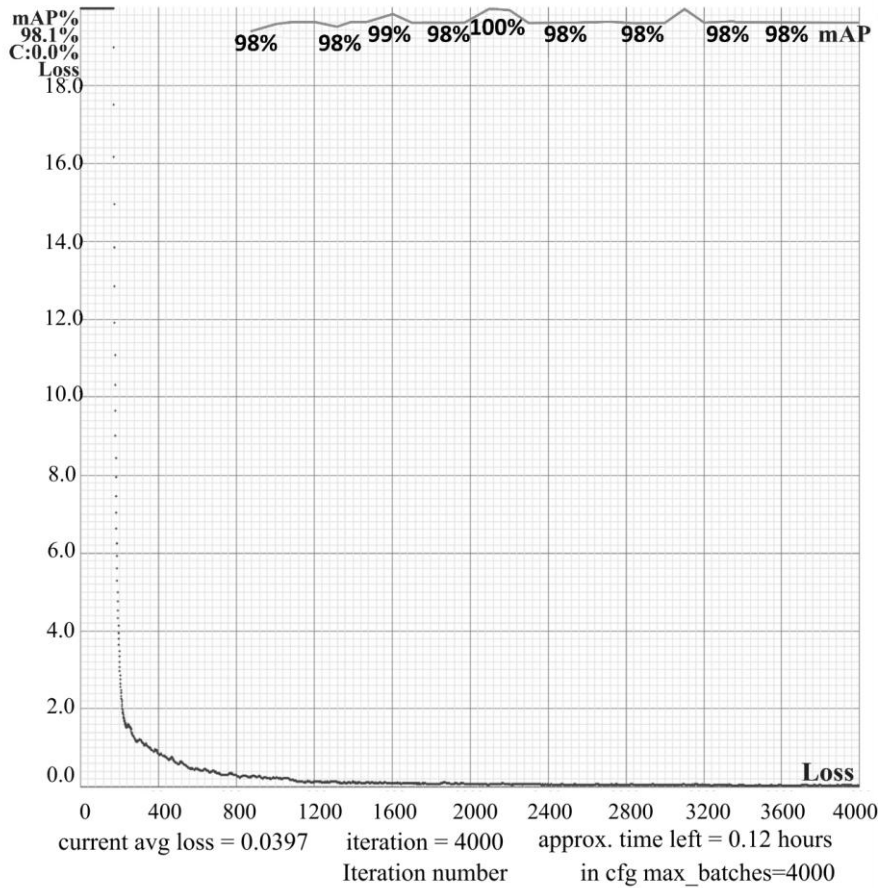

Figure 9. Accuracy and loss values for various epoch in testing set 2 – stained images

Table X. YOLO Architecture

Layer	Kernel, Stride	Output Shape
Conv2D	(3,3), 1	(448, 448, 16)
MaxPool	(2,2), 2	(224, 224, 16)
Conv2D	(3,3), 1	(224, 224, 32)
MaxPool	(2,2), 2	(112, 112, 32)
Conv2D	(3,3), 1	(112, 112, 64)
MaxPool	(2,2), 2	(56, 56, 64)
Conv2D	(3,3), 1	(56, 56, 128)
MaxPool	(2,2), 2	(28, 28, 128)
Conv2D	(3,3), 1	(28, 28, 256)
MaxPool	(2,2), 2	(14, 14, 256)
Conv2D	(3,3), 1	(14, 14, 512)
MaxPool	(2,2), 1	(7, 7, 512)
Conv2D	(3,3), 1	(7, 7, 1024)
Conv2D	(3,3), 1	(7, 7, 1024)
Conv2D	(1,1), 1	(7, 7, 125)

Furthermore, we improved the developed model with the You Only Look Once (YOLO) v3 algorithm [25] using DarkNet-53 framework. In this experiment, the input layer was a typical CNN which had convolutional layers and max-pooling layers. The detailed construction of the YOLO architecture is described in Table X.

We also conducted several experiments using various epoch sizes as depicted in Figs. 8 and. 9. It is shown in Fig. 8 that the average loss value of the system was 0.0833 with 87% highest accuracy value for testing set 1. Testing set 1 consisted of untrained and unstained white blood cell images. Fig. 9 shows the accuracy and loss values for various epochs in testing set 2. The white blood cell images in testing set 2 were previously colored with Wright stain. It is shown in Fig. 9 that the loss value of the system was 0.0397 with 100% highest accuracy value. The major contribution of this research is that the developed model could give high recognition results of white blood cells from unstained images, which are barely recognized by the human eye.

Finally, the samples of correct detection of white blood cells are shown in Fig. 10. Figs. 10 (a) and 10(b) show a pair of images showing blood cells at the same location, while Figs. 10(c) and 10(d) show another pair for color-stained and unstained conditions. The green rectangle in each image in Fig. 10 marks the white blood cell areas detected by the developed system.

On the contrary, Fig. 11 shows incorrect detections by the system towing to noise existence. The figure further shows paired images for both stained and unstained images of the same blood cells areas. Based on Figs. 11(a) and 11(b), it can be seen that the pair of images produced false detection results. The same observation is present in the pairs in Figs. 11(c) and 11(d). The cause of detection errors in unstained images is because the cells could not be seen clearly by the human eye. However, the stained images show some noise spots for each detected area, which are most likely the cause of incorrect detection.
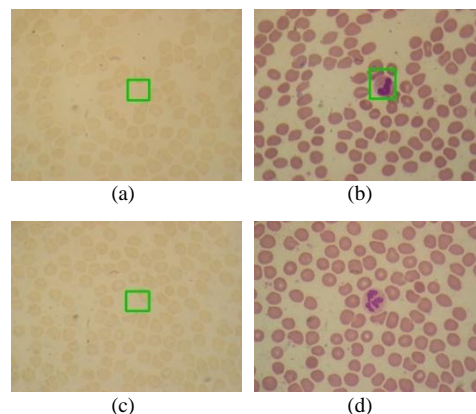

Figure 10. Samples of correct white blood cells detection (shown in pairs a-b and c-d)
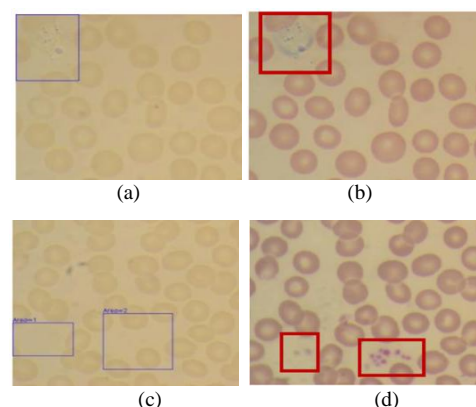

Figure 11. Incorrect detections of white blood cells towing to noise existence (shown in pairs a-b and c-d)

IV. CONCLUSION

This study initiates the elimination of the use of color-stained images in a white blood cell detection system. The staining process itself is time-consuming and inefficient. Therefore, an automatic white blood cell detection system from unstained images was developed, and a modification of the watershed segmentation method was applied to the developed system to locate the white blood cells areas from unstained images. Several experiments were conducted on the unstained images and the results were compared with that of the stained images. Experimental results showed that the proposed system using the modified watershed method achieved 65.42% detection accuracy for detecting the white blood cells from the unstained images, while 94.82% detection accuracy was achieved for color-stained images. Other experiments were also conducted with the CNN method for comparison. In these experiments, the system obtained 65.33% and 74.85% detection accuracies for the unstained images and the color-stained images, respectively. Based on the experimental results, it can be concluded that the developed system provides an effective means of performing blood cells detection without requiring the use of color-stained images.

In the future, several improvements, such as the use of dynamic parameters for thresholding, the application of sharpening functions for enhancing the image texture, and the use of various layer configurations and hyperparameters in neural network methods will be considered.

REFERENCES

[1] J.P. Duan and L. Yu, "A WBC segmentation method based on HSI color space", *2011 4th IEEE International Conference on Broadband Network and Multimedia Technology*, pp.629-632, 2011.

[2] L. Lina, A. Chris. and B. Mulyawan, "Focused color intersection for leukocyte detection and recognition system", *International Journal of Information and Electronics Engineering*, Vol. 3, No. 5, pp.498-501, 2013.

[3] L. Lina, A. Chris., B. Mulyawan., and A.B. Dharmawan, "A leukocyte detection system using scale invariant feature transform method", *International Journal of Computer Theory and Engineering*, Vol. 8, No. 1, pp.69-73. 2016.

[4] S.N. Safuan, M.R Tomari, and W.N. Zakaria, "White blood cell (WBC) counting analysis in blood smear images using various color segmentation methods", *Measurement*, Vol. 116, pp.543-555, 2018.

[5] S. Alférez, Merino, Acevedo A., L. Puigví, and J. Rodellar, "Color clustering segmentation framework for image analysis of malignant lymphoid cells in peripheral blood", *Medical & Biological Engineering & Computing*, Vol. 57, pp.1265-1283, 2019.

[6] G. Poshamallu, "Binary image processing implementation on fpga using morphological dilation and erosion techniques", *International Journal of Engineering Science and Computing*, Vol. 6, No. 4, pp.4280-4283, 2016.

[7] N.M. Sobhy, N.M. Salem, and M.E. Dosoky, "A comparative study of white blood cells segmentation using otsu threshold and watershed transformation", *Journal of Biomedical Engineering and Medical Imaging*, Vol. 3, No. 3, pp.15-24, 2016.

[8] K. Al-Dulaimi, V. Chandran, J. Banks, I. Tomeo-Reyes, and K. Nguyen, "Classification of white blood cells using bispectral invariant features of nuclei shape", *2018 Digital Image Computing: Techniques and Applications (DICTA)*, pp.1-8, 2018.

[9] A. Merino, L. Puigví, L. Boldú, S. Alférez, and J. Rodellar, "Optimizing morphology through blood cell image analysis", *International Journal of Laboratory Hematology*, Vol. 40, No. 1, pp.54 – 61, 2018.

[10] L.N. Mahdy, K.A. Ezzat, A. Darwish, and A. Hassanien, "Automatic counting of infected white blood cells using multi-level thresholding", *2019 Ninth International Conference on Intelligent Computing and Information Systems (ICICIS)*, pp.141-146, 2019

[11] J. Rodellar, S. Alférez, A. Acevedo, Á. Molina, and A. Merino, "Image processing and machine learning in the morphological analysis of blood cells", *International Journal of Laboratory Hematology*, Vol. 40, No. 1, pp.46 – 53, 2018.

[12] R. Chu, X. Zeng, L. Han, and M. Wang, "Subimage cosegmentation in a single white blood cell image", *2015 7th International Conference on Computational Intelligence Communication Systems and Networks*, pp.152-157, 2015.

[13] C.D. Ruberto, A. Loddo, and L. Putzu, "Detection of red and white blood cells from microscopic blood images using a region proposal approach", *Computers in Biology and Medicine*, 116, 103530, 2020.

[14] K. Sudha and P. Geetha, "Leukocyte segmentation in peripheral blood images using a novel edge strength cue-based location detection method", *Medical & Biological Engineering & Computing*, Vol. 58, pp.1995 – 2008, 2020.

[15] F. Qin, N. Gao, Y. Peng, Z. Wu, S. Shen, and A. Grudtsin, "Fine-grained leukocyte classification with deep residual learning for microscopic images", *Computer Methods and Programs in Biomedicine*, Vol. 162, pp.243-252, 2018.

[16] L.H.S. Vogado, R.M.S. Veras, F.H.D. Araújo, R.R.V Silva, and K.R.T Aires, "Leukemia diagnosis in blood slides using transfer learning in CNNs and SVM for classification", *Engineering Applications of Artificial Intelligence*, Vol. 72, pp.415-422, 2018.

[17] N. Ahmed, A. Yigit, Z. Isik, and A. Alpkocak, "Identification of leukemia subtypes from microscopic images using convolutional neural network", *Diagnostics*, Vol. 9, No. 3, pp.104, 2019.

[18] A. Acevedo, S. Alférez, A. Merino, L. Puigví, and J. Rodellar, "Recognition of peripheral blood cell images using convolutional neural networks", *Computer Methods and Programs in Biomedicine*, *180*, 105020, 2019.

[19] R.B Hegde, K. Prasad, H. Hebbar, and B.M Singh, "Comparison of traditional image processing and deep learning approaches for classification of white blood cells in peripheral blood smear images", *Biocybernetics and Biomedical Engineering*, Vol. 39, No. 2, pp.382-392, 2019.

[20] L. Ma, R. Shuai, X. Ran, W. Liu, and C. Ye, "Combining DC-GAN with ResNet for blood cell image classification", *Medical & Biological Engineering & Computing*, Vol. 58, pp.1251-1264, 2020.

[21] S. Nurmaini, A.E. Tondas, R.U. Partan, M.N. Rachmatullah, A. Darmawahyuni, F. Firdaus, B. Tutuko, R. Hidayat, and A.I. Sapitri, "Automated detection of COVID-19 infected lesion on computer tomography images using faster-RCNNs", *Engineering Letters*, Vol. 28, No. 4, pp. 1295-1301, 2020.

[22] A. M. Ceballos-Arroyo, S. Robles-Serrano, and G. Sanchez-Torres, "A morphological convolutional autoencoder for segmenting pigmented skin lesions", *Engineering Letters*, Vol. 28, No. 3, pp. 855-866, 2020.

[23] H. Kutlu, E. Avci, and F. Ozyurt, "White blood cells detection and classification based on regional convolutional neural networks", *Medical Hypotheses*, Vol. 135, No. 10, 109472, 2020.

[24] Q. Wang, S. Bi, M. Sun, Y. Wang, D. Wang, and S. Yang, "Deep learning approach to peripheral leukocyte recognition", *PLoS ONE*, Vol. 14, No. 6, e0218808, 2019.

[25] A. Mujahid, M.J. Awan, A. Yasin, M.A. Mohammed, R. Damasevicius, R. Maskeliunas, and K.H. Abdulkareem, "Real-time Hand Gesture recognition based on Deep Learning YOLOv3 Model", *Applied Sciences*, Vol. 11, No. 9, 4164, 2021.

Lina Lina is an Associate Professor of the Computer Science department at Tarumanagara University in Jakarta, Indonesia. In 2009, she obtained a Ph.D. degree from Nagoya University – Japan. Currently, she is the head of the Pattern Recognition research laboratory at Tarumanagara University. She is also a member of IEEE, IEICE, and IAENG. Her research interests are in pattern recognition and intelligent systems.

David Reynaldo is a research assistant of the Pattern Recognition research laboratory, Computer Science department, Tarumanagara University in Jakarta, Indonesia. He obtained his bachelor's degree from Tarumanagara University in 2019.

Danny Danny is a research assistant of the Pattern Recognition research laboratory, Computer Science department, Tarumanagara University in Jakarta, Indonesia. He obtained his bachelor's degree from Tarumanagara University in 2021.

Arlends Chris is an Assistant Professor of the Medical Faculty, Tarumanagara University in Jakarta, Indonesia. He obtained his Ph.D. degree from Universitas Negri Jakarta, Indonesia in 2019. His main research interests lie in biomedical engineering and technology-based education.